This is a repository copy of *Non-Functionalized Ultrasmall Silica Nanoparticles Directly and Size-Selectively Activate T Cells*.

White Rose Research Online URL for this paper:
http://eprints.whiterose.ac.uk/139449/

Version: Accepted Version

Non-Functionalized Ultrasmall Silica Nanoparticles Directly and Size-Selectively Activate T Cells

Authors: Bradley Vis[†‡§*], Rachel E. Hewitt[†‡*], Nuno Faria[†‡], Carlos Bastos[†‡], Helen Chappell[‡Φ], Laetitia Pele[†‡], Ravin Jugdaohsingh[†‡], Stephen D. Kinrade[§], Jonathan J. Powell[†‡]

[†]Biomineral Research Group, Department of Veterinary Medicine, University of Cambridge, Madingley Road, Cambridge CB3 0ES, UK.

[‡]Biomineral Research Group, Department of Mineral Science and Technology, MRC Elsie Widdowson Laboratory, Fulbourn Road, Cambridge CB1 9NL, UK.

[§]Department of Chemistry, Lakehead University, Thunder Bay, Ontario P7B 5E1, Canada.

[Φ]School of Food Science and Nutrition, University of Leeds, Woodhouse Lane, Leeds, LS2 9JT, UK

*Equal contributors

Corresponding author: Jonathan Powell. jjp37@cam.ac.uk

Abstract

Sub-micron sized silica nanoparticles, even as small as 10-20 nm in diameter, are well known for their activation of mononuclear phagocytes. In contrast, the cellular impact of those < 10 nm (i.e., ultrasmall silica nanoparticles (USSN)) is not well established for any cell type despite anticipated human exposure. Here, we synthesized discrete populations of USSN, with volume median diameters between 1.8 to 16 nm, and investigated their impact on the mixed cell population of human primary peripheral mononuclear cells. USSN of 1.8-7.6 nm diameter, optimally 3.6-5.1 nm diameter, induced dose-dependent CD4 and CD8 T cell activation in terms of cell surface CD25 and CD69 upregulation at concentrations above 150 μM Si_{TOTAL} (~500 nM particles). Induced activation with only ~2.4 μM particles was (a) equivalent to that observed with typical positive control levels of Staphylococcal enterotoxin B (SEB) and (b) evident in antigen presenting cell-deplete cultures as well as in a pure T cell line (Jurkat) culture. In the primary mixed cell population, USSN induced IFN-γ secretion but failed to induce T cell proliferation or secretion of IL-2, IL-10, or IL-4. Collectively, these data indicate that USSN initiate activation, with Th_1-polarisation, of T cells via direct particle-cell interaction. Finally, similarly sized iron hydroxide particles did not induce expression of T cell activation markers, indicating some selectivity of the ultrasmall particle type. Given that humans may be exposed to ultrasmall particles, and that these materials have emerging bio-clinical applications, their off-target immunomodulatory effects via direct T cell activation should be carefully considered.
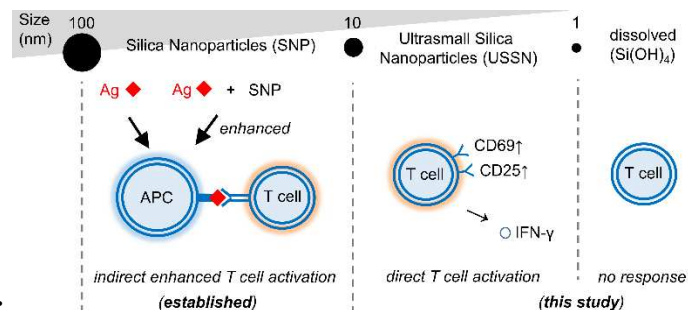
Table of Contents graphic:

Keywords: T cells, activation, ultrasmall, silica, nanoparticles, CD25, CD69

Nanoparticles that are 1-10 nm in diameter are termed ultrasmall and are attracting significant attention for clinical applications.[1-4] They have desirable optical, magnetic and quantum confinement properties as well as the ability to distribute widely in tissue.[5] Ultrasmall silica nanoparticles (USSN) are of particular interest due to their tailorable properties and biocompatibility.[5] Whilst functionalized USSN are being developed for bio-clinical applications, currently most human exposure is likely to be to non-functionalized silica nanoparticles. For example, the average UK adult ingests 35 mg silicate particles daily in the form of excipients and food additives and, although these are predominately >200 nm in diameter, studies have suggested that primary particles of silica <10 nm can be released during the digestion process.[6,7] Exposure to amorphous silicates via the lungs is also frequent, in the form of environmental dusts or personal hygiene products such as dry shampoo, and other sources such as toners and varnishes.[8,9] The impact of inhaled amorphous silica and whether it further fractionates, as appears to be the case in the gut, is not well understood.[10]

The interaction of silica particles of 10-1000 nm diameter with mammalian cells has been extensively studied.[11] In addition to inducing phagocytic inflammation,[12,13] silica nanoparticles have been shown to enhance adaptive immunity by increasing cross presentation of co-administered protein antigen by antigen presenting cells, and they also act synergistically with bacterial constituents to enhance T cell responses.[14-16] Humoral immunity has also been found to increase with silica exposure, as SNP-treated animals show greater immunoglobulin responses to co-administered protein antigen compared to the non-silica-treated controls.[17,18] Although such cellular responses to silica particles are established, the impact of the much smaller fraction (i.e., USSN) remains unknown in spite of potential human exposure and emerging clinical applications.[7,19] Here, we investigated the response of primary human peripheral blood mononuclear cells (PBMC) to a range of sub-10 nm diameter amorphous silica particles plus a 16 nm silica comparator (i.e., non-USSN), all synthesized through size-selective aqueous methods.

Results/Discussion

Characterization of USSN dispersions

USSN dispersions were generated through the precipitation of orthosilicic acid ($Si(OH)_4$). Orthosilicic acid exhibits significantly reduced solubility below pH 9 and, when concentration, pH and ionic strength are carefully controlled, it self-associates to form USSN that are metastable under physiological conditions.[20] A dispersion with a median particle diameter of 3.6 ± 0.5 nm was prepared by pH-neutralizing an alkaline silicate solution of ca. 23 mM Si and incubating it at room temperature for 12-24 h (Figure 1a).

Silicon-29 NMR spectroscopy was used to determine the extent of silicate condensation for an identical USSN dispersion prepared from ^{29}Si-enriched (99.35 atom%) materials (Figure 1b, Table 1). Amorphous silica, whose long-range formula is SiO_2, consists of tetraoxosilicon centres (denoted Q for quadrifunctional) interlinked by siloxane bonds.[21] A fully condensed Si centre (Q^4, being linked to 4 other centres) can only exist in the core of a particle, whereas partially condensed centres (Q^2 or Q^3) are associated with the surface. USSN accounted for most ($84 \pm 3\%$) of the silicon content in the dispersion and, of this, 43% was partially condensed (Q^2 & Q^3) and 57% was fully condensed (Q^4). The remaining Si content was comprised of aqueous monomeric (Q^0) and dimeric (Q^1-Q^1) silicic acid molecules.[22-24]

Table 1. Silicon distribution in the dispersion, as determined by integration of the ^{29}Si NMR spectrum; Q^n represents a Si atom with n coordinated −OSi groups

Overall Si distribution		USSN Si distribution	
Q^0, Q^1 (dissolved)	Q^2, Q^3, Q^4 (USSN)	Q^2, Q^3 (surface)	Q^4 (core)
$16 \pm 3\%$	$84 \pm 3\%$	$43 \pm 2\%$	$57 \pm 2\%$

A significant fraction of the terminal hydroxyl groups (residing at partially condensed Si centres) on USSN is deprotonated at physiological pH, as evidenced by USSN's negative zeta-potential both in the stock dispersion at pH 7.1 (Figure 1c) and in the more complex media, namely PBS and RPMI (Table S1). Inexorably, therefore, any USSN encountered by cells would be negatively charged.

USSN with a median hydrodynamic diameter of 3.6 ± 0.5 nm were calculated to contain 330 ± 62 Si atoms, assuming a hydration shell of 0.2-0.6 nm and an amorphous silica density of 1.90 g/cm^3.[25] This Si packing density is in agreement with that obtained by manual addition of small energy-minimized silica clusters[26] to construct a 2.9 nm hydration shell-deficient particle (Figure S1) and also with values reported in the literature (22-29 $\underline{Q}^4$ centres/nm^3).[27] Based on these data, and the NMR analyses above, a dispersion of 3.6 nm USSN at 1 mM Si_{TOTAL} approximates to a 3 μM particle concentration.

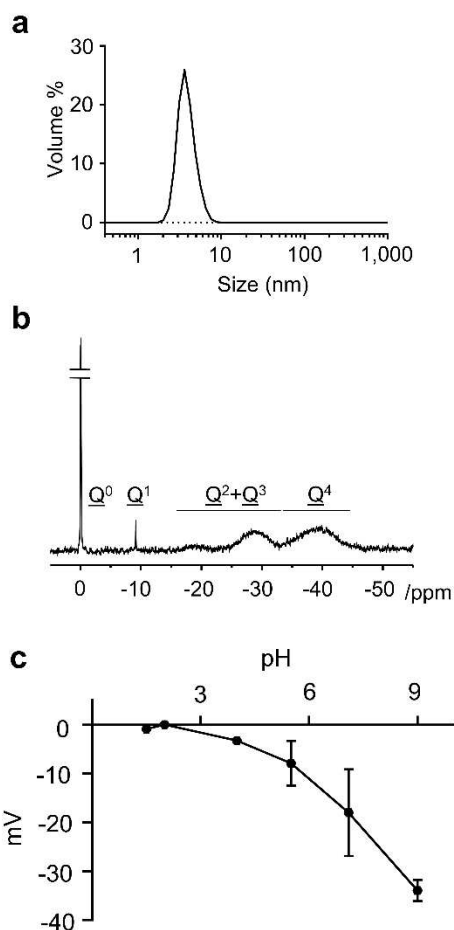**Figure 1. Physical characterization of USSN. a**. Particle size distribution of a USSN dispersion (ca. 23 mM Si, pH 7, incubated 15 h) **b.** Silicon-29 NMR spectrum of an equivalent USSN dispersion that is enriched 99.35 atom% in ^{29}Si. The signal corresponding to orthosilicic acid ($\underline{Q}^0$) is set to 0 ppm. **c.** pH-dependence of USSN zeta-potential in UHP water (mean ± SD).

Cellular responses to USSN dispersions

The effect of USSN on PBMC viability was investigated. USSN of 3.6 ± 0.5 nm median diameter were added to tissue culture media at 150-800 μM Si_{TOTAL} (ca. 0.5-2.4 μM particles) and the viability of monocyte, B and T lymphocyte cell subsets was examined after 24 h incubation. The percentage of viable monocytes and B cells decreased in a dose-dependent fashion, with significant reduction being evident at 300 μM Si_{TOTAL} (Figure 2). The viability of T cells also decreased, although their tolerance to USSN was greater than that of B cells or monocytes, possibly due to differences in particle uptake and intracellular loading.[12,28] Orthosilicic acid, over the same Si_{TOTAL} concentration range, had no effect on cell viability (data not shown).

Having established sub-lethal concentrations of USSN, we next examined transcriptional responses of PBMCs to the particles (at 150 μM Si_{TOTAL}). Consistent with established pro-inflammatory responses towards larger silica particles,[12,13] multiple gene groups that are associated with inflammation were upregulated in response to USSN (Tables S2 and S3) – including latent infection of homo sapiens with Mycobacterium tuberculosis (30 genes), P75NTR signals via NFκB (15 genes), KEGG rheumatoid arthritis (86 genes) and WP530 cytokines and inflammatory response (23 genes). Indeed, modest inflammasome activation by USSN was confirmed through LPS priming of PBMC and then chasing with USSN at three concentrations. USSN enhanced IL-1β protein secretion beyond vehicle alone, corroborating previous studies with larger particles,[15] albeit not to the same extent as the positive control (insoluble peptidoglycan from Staphylococcus aureus: Figure S2).[29]

Immune CEll POPulation analyses (ICEPOP), as developed by Wijaya et al. to identify responding cell types in mixed cell cultures,[30,31] revealed that classical phagocytic cells (dendritic cells and especially monocytes) were the subtypes most significantly affected by USSN (Figure 2b and Table 2). These cells are well known to respond to SNP > 10 nm diameter,[12,15] and hence our data demonstrate that phagocyte responsiveness also extends to USSN despite the small particles size. It is likely that these cells have other endocytic uptake mechanisms in addition to classical phagocytosis of larger particles. For natural killer

6

(NK) cells a lesser but still significant response was also observed when the mixed cell culture was challenged with USSN (Figure 2b and Table 2). However, these cells respond non-specifically to danger signals,[32,33] and typically to inflammatory signalling, just as we observed here for the PBMC challenge with USSN (see above). For B cells, the responses of all gene groups barely rose above the threshold for significance when the PBMC were exposed to USSN (Figure 2b). At the single gene level, however, two B cell-specific genes were significantly up-regulated (Table 2), consistent with B cells having endocytic/phagocytic capability and with the known effect of larger SNP in enhancing B cell antigen responses.[17,18] Finally, T cells, which are not known to take up particles or to respond non-specifically to danger signals,[12,38] demonstrated an unanticipated reaction to USSN challenge. In particular, the response of gene groups associated with 12 hour activated Th_1 T cells and with memory T cells (resting and activated) were clearly enhanced above the no response cell threshold (Figure 2b). Two genes, which the ICEPOP algorithm considers specific to T cells (ICOS, ZBED2),[34] were upregulated by USSN. Other genes with an expression typically associated with T cells, albeit not entirely specifically so, were also upregulated by USSN. For example, genes which commonly correspond to T cell signalling (ly9) as well as to activation of cytotoxic and helper T cells (CRTAM, CD69, IFN-γ, XCL1) had increased expression after USSN treatment.[35-37]
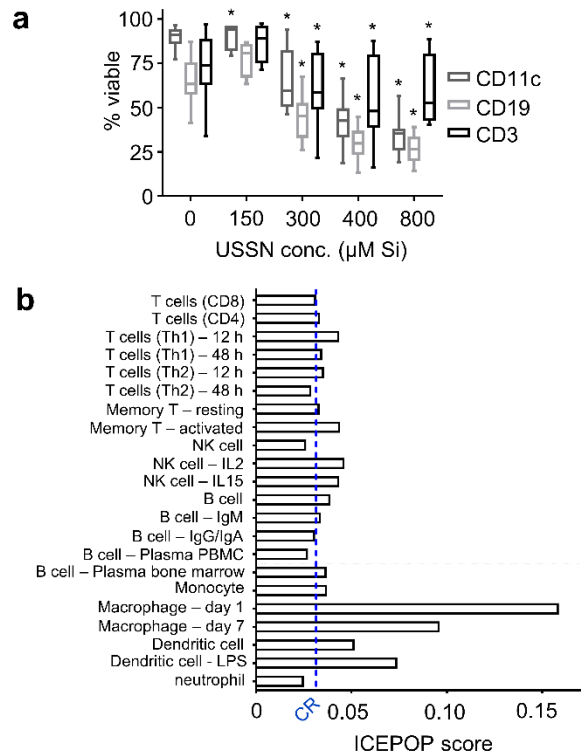
Figure 2. The cellular activity of USSN on primary peripheral cells. a. The effect of USSN on monocyte (CD11c), B cell (CD19) and T cell (CD3) viability in PBMC culture at 24 h. (* denotes significance compared to the control, two-tailed paired T-test, $p < 0.05$, n = 4-18.) **b.** Response of specific cell subtypes to 150 μM USSN as identified using Immune CEll POPulation (ICEPOP) analysis of gene expression data (n=3). Values above the cell type response threshold (CR) indicate cell subtype responders and the length of the histogram (ICEPOP score) denotes the extent of this response.

Table 2. The up-regulatory effect of 150 μM USSN on the expression of genes associated specifically with monocytes, dendritic cells, B cells, NK cells and T cells; genes were identified by Abbas et al.[34]

Cell type	Up-regulated genes
Monocyte	CCRL2, CTSD, CTSL, CXCL5, DFNA5, GJB2, GPR84, IL1RN, IL24, MMP19, NPC1, NRIP3, PLAUR, PLD1, SNX9, ZFYVE16
Dendritic cells	CHST7, NR4A3, RAB9A, TTYH2
B cells	EIF2AK3, ELL2
NK cells	TGFBR1
T cells	ICOS, ZBED2

8

These findings raised the possibility that USSN could activate T cells. We therefore sought confirmation at the protein level using cell membrane markers of T cell activation. CD25 is a component of the IL-2 receptor and is involved in late-stage T cell proliferation and differentiation.[39,40] CD69 is an earlier and more sensitive marker of T cell activation, and is involved in cytotoxic function as well as in T cell migration and retention.[35,41,42] USSN, at 150-800 μM Si_{TOTAL} (ca. 0.5-2.4 μM particles), significantly induced both cell surface markers on primary human CD4 and CD8 T cells of PBMCs in a dose-dependent fashion. At the highest USSN dose, the effects were equivalent to those induced by typical 'positive control' levels of superantigen Staphylococcal enterotoxin B (SEB), both in terms of percentage positive cells (Figure 3a-3b) and fluorescence intensity (Figure 3c-3d). Non-particulate silica (i.e., orthosilicic acid) at the same concentrations had no effect. USSN determinants of T cell viability and T cell activation appeared to be unrelated. At 150 μM Si_{TOTAL}, for example, there was significantly increased expression and fluorescence intensity of CD69 on CD4 and CD8 T cells, as well as enhanced fluorescence intensity of CD25 on CD8 T cells, whereas viability of these cells was unaffected. Moreover, USSN-induced upregulation of CD25/69 followed a dose-dependent sigmoidal curve (r^2 = 0.686-0.882, Figure 3a-d). USSN-induced T cell death was not dose-dependent (r^2 = 0.18, Figure 2a), by contrast.
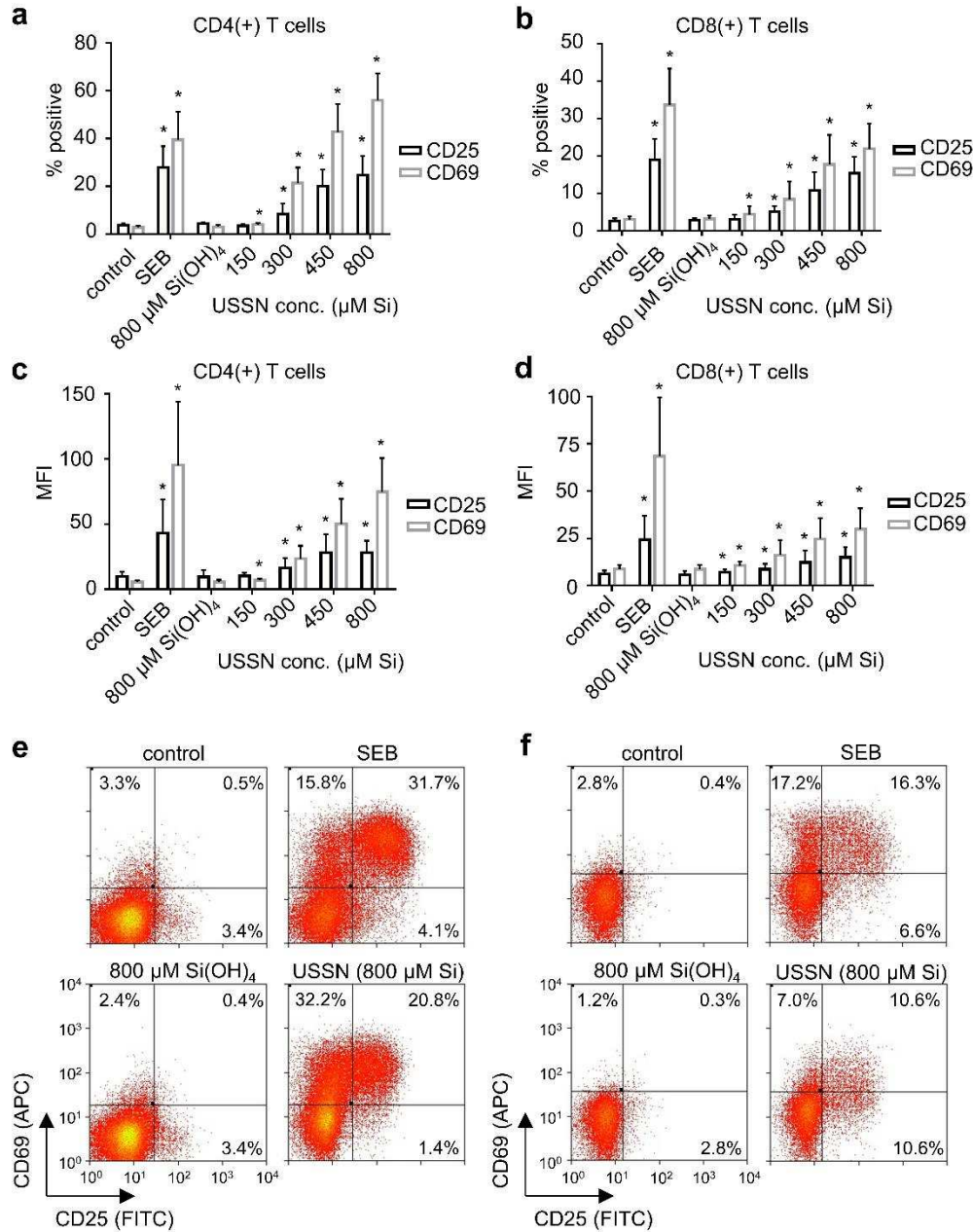
Figure 3. The cellular activity of USSN on primary T cells. The effect of SEB, orthosilicic acid (Si(OH)$_4$) and USSN on the percentage of CD4 (**a.**) and CD8 (**b.**) T cells that are positive for CD25 and CD69 in PBMC culture after 24 h. The effect of SEB, orthosilicic acid and USSN on the mean fluorescence intensity (MFI) of CD25 and CD69 on CD4 (**c.**) and CD8 (**d.**) T cells in PBMC culture after 24 h. Data shown represent the mean ± standard deviation for ≥7 donors. (* denotes significance compared to the control, two-tailed paired T-test, p < 0.05.) Representative bivariate dot plots show expression of CD25 and CD69 on CD4 (**e.**) and CD8 (**f.**) T cells. The percentage of cells positive for CD25 and CD69 followed a dose-dependent sigmoidal curve (r^2 = 0.75 and 0.88, respectively, for CD4 T cells and 0.72 and 0.69, respectively, for CD8 cells).

We next investigated whether CD4 or CD8 T cells proliferated in response to USSN. In marked contrast to the SEB positive control, USSN, induced minimal proliferation of either CD4 or CD8 T cells following 3 or 5 days of culture (Figure 4a-d) at levels that stimulated high T cell expression of CD69 and CD25. In corroboration, IL-2, a cytokine essentially involved in late-stage T cell proliferation, was significantly secreted at days 1, 3 and 5 by cells challenged with SEB but was only present at, or close to, baseline levels in the supernatants of cells exposed to USSN (Figure 5a).

Thus, USSN induced markers of T cell activation, but only minimal proliferation. Next, therefore, by measuring classical T cell-derived cytokines from PBMC challenged with USSN, we considered the possible role of these activated-but-non-proliferating T cells in the development of T helper cell responses by assessing cytokine levels associated with regulation (IL-10), Th_1 (IFN-γ) or Th_2 (IL-4) phenotypes.[43,44] Positive control SEB induced all three cytokines, but IFN-γ secretion was dominant. USSN failed to stimulate IL-4 and IL-10, but induced IFN-γ in a dose-responding fashion despite the lack of T cell proliferation (Figure 5b-d).
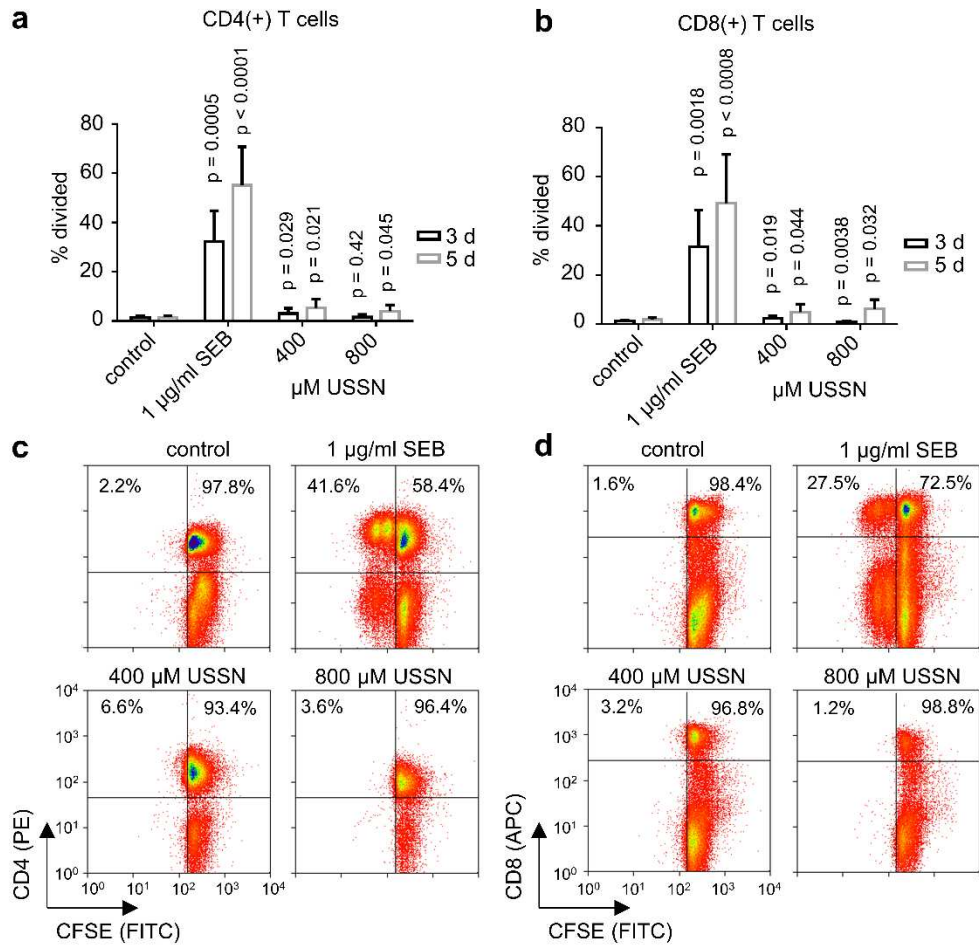
Figure 4. The impact of USSN on primary T cell proliferation. The effect of SEB and USSN on the percentage of divided (CFSE dilute) CD4 (**a.**) and CD8 (**b.**) T cells in PBMC culture after 3 d and 5 d. Data shown represent the mean ± standard deviation for 7 donors (p-values show differences compared to the control, two-tailed paired T-tests). Representative bivariate dot plots show CFSE intensity of CD4 (**c.**) and CD8 (**d.**) T cells
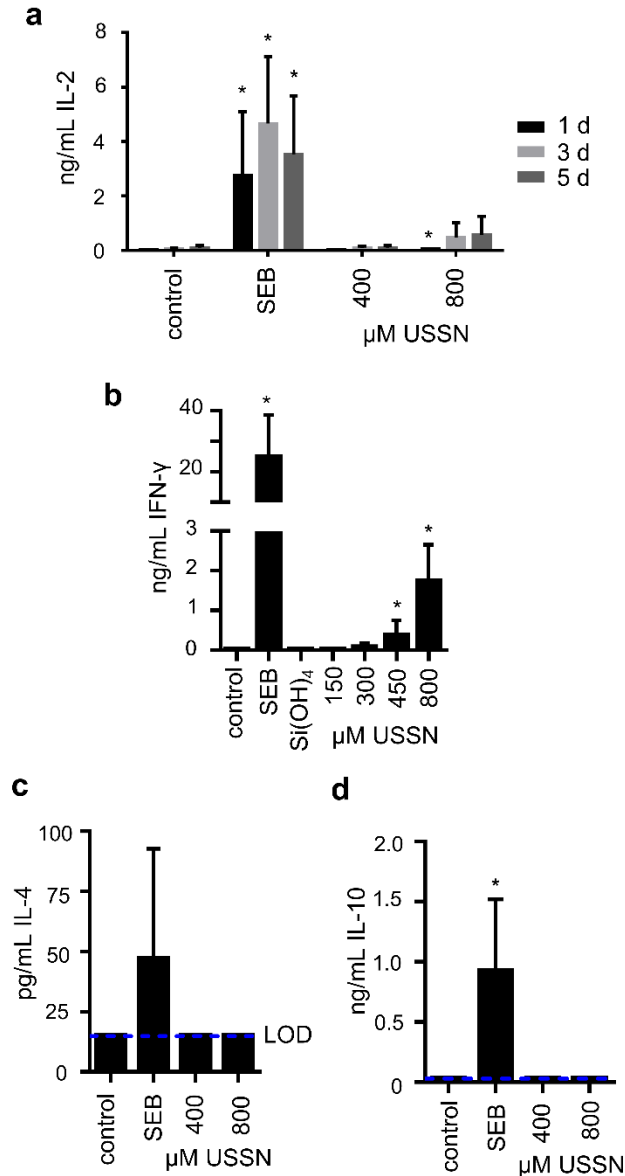
Figure 5. The impact of USSN on cytokine levels in supernatants of primary PBMC cultures. The effect of SEB and USSN on IL-2 (**a.**), IFN-γ (**b.**), IL-4 (**c.**) and IL-10 (**d.**) levels in PBMC culture supernatants. IL-2 levels were assessed after 1 d, 3 d and 5 d incubations. IFN-γ, IL-4 and IL-10 levels were assessed after 1 d incubation. Data shown represent the mean ± standard deviation for ≥ 5 donors. (* denotes significance compared to the control, two-tailed paired T-test, $p < 0.05$.)

Next we considered whether USSN size was critical for initiation of T cell activation. Most nanoparticles are unstable in complex media, readily interacting with protein and/or forming aggregates.[45,46] Additionally, USSN will dissolve when diluted below the solubility limit of silicic acid (ca. 1.7 mM Si).[21] Ultrafiltration

and elemental analysis (Figure 6a and S3) revealed that, indeed, the phase distribution of the 3.6 nm USSN stock dispersion changed after dilution to 800 μM Si_{TOTAL} in tissue culture medium. Within 30 minutes of dilution, ca. 25% of the particles had agglomerated (into clusters with a diameter greater than 11 nm) and ca. 35% had dissolved (Figure 6a). The large agglomerated fraction was unchanged after an hour, but percent dissolution had increased. Finally, by 8 h, nearly all the USSN had dissolved (Figure S3). These results imply that (a) USSN would have relatively short-lived encounters with cells, and (b) the size responsible for inducing T cell activation is uncertain. We therefore generated five stock suspensions with narrow size distributions and median diameters ranging from 1.8 ± 0.7 to 16 ± 1.3 nm (Figure 6b), using pH, Si concentration and salinity to tailor particle growth (see Methods). After 24 h exposure, only the 16 nm particles failed to elicit T cell activation in PBMC cultures, whereas all ultrasmall particles were effective; optimal activation, adjudged by CD25 and CD69 expression, occurred with USSN of 3.6-5.1 nm diameter (Figure 6c,d). Dissolution over time in simple aqueous media, mimicking that in cell culture, indicated that cell encounters with USSN of 1.8 ± 0.7 nm diameter would be much briefer than those involving larger particles (Figure 6e), which would suggest that the decreased efficacy of the smallest particles could be due to their size, short lifetime, or both. Given the differing dissolution profiles of the dispersions, the overlap in size distribution as measured in the stock solutions, and the alterations to particle size in complex media, the exact identity of the 'on-target' particle size(s) responsible for cell activation is not known. Notwithstanding, our results demonstrate that only silica nanoparticles that start out in the ultrasmall size range (i.e., < 10 nm in diameter) are capable of inducing significant T cell activation and, with our methods of particle preparation, optimally so at 3.6-5.1 nm.
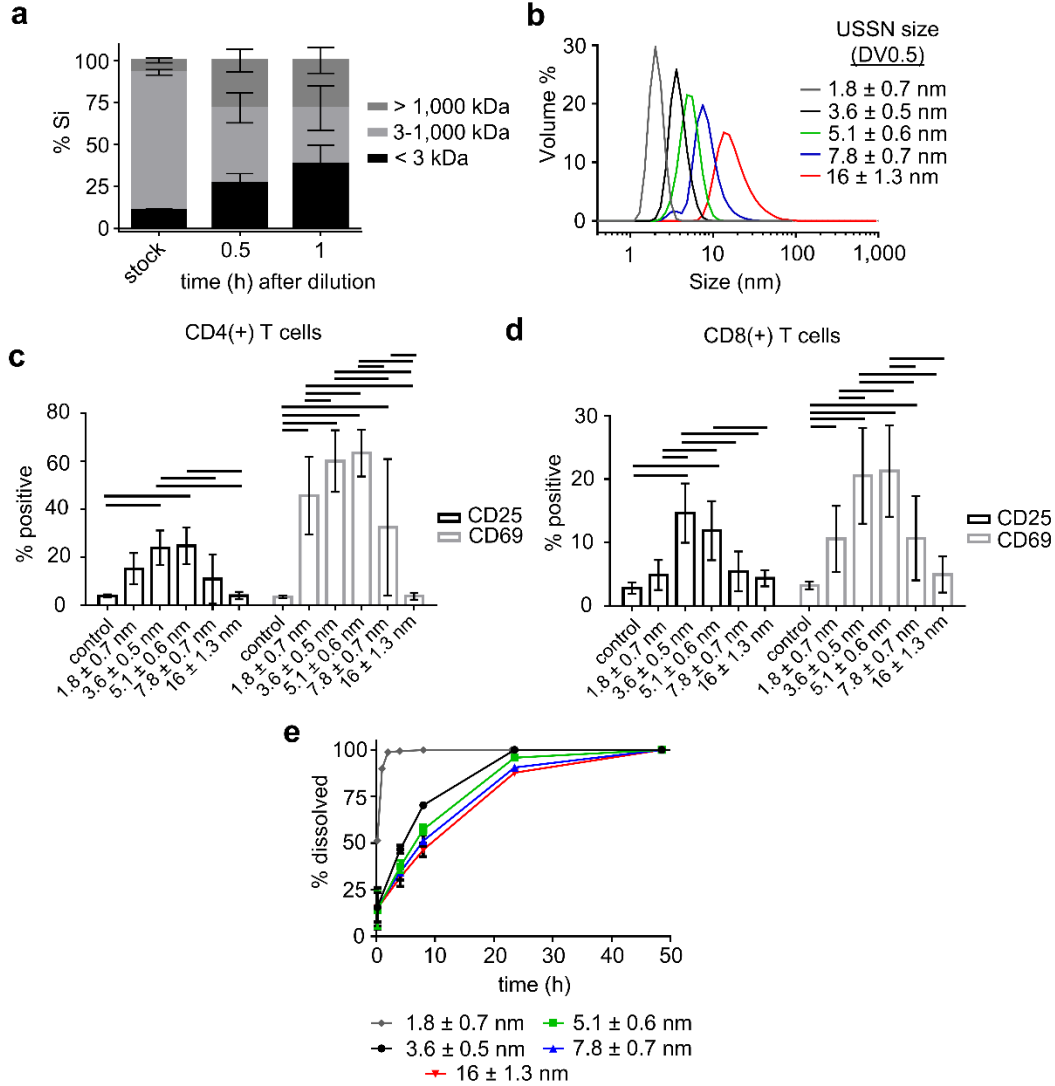
Figure 6. Size-dependent properties of the USSN dispersions and their effect on induced T cell activation. a. Percentage of silicon that passed through 3 and/or 1,000 kDa ultrafilters in USSN dispersions (ca. 23 mM, pH 7, 15 h) and after dilution to 800 μM Si and incubation at 37 °C in RPMI + 10% FBS media for 0-1 h. **b.** Particle size distribution for tailored USSN dispersions (20-40 mM Si), mainly through differential saline addition, after 24 h incubation at room temperature. **c-d**. Expression of CD25 and CD69 on CD4 and CD8 T cells in PBMC cultures treated with USSN dispersions of different particle sizes after 24 h. Data shown represent the means ± standard deviation for a minimum of 8 donors. Lines denote a statistically significant difference (2-way ANOVA, p<0.05). **e.** Effect of USSN size on dissolution rate after dilution to ca. 1 mM Si in HEPES buffer (pH 7.0-7.3)

We next investigated whether USSN induced T cell activation directly or indirectly. Previous studies have

shown that silica nanoparticles larger than USSN are able to (i) promote cross-presentation of exogenously

15

derived antigen by antigen presenting cells (APCs), thereby enhancing the activity of matched (i.e., antigen-specific) responder CD8^{+} T cells,[14] and (ii) act synergistically with bacterial-derived components to increase T cell activation.[15,16] In our experiments, however, bacterial components were lacking, given the normal, sterile cell culture environment. Similarly, exogenous antigen and antigen specific T cells were not added, and primary peripheral blood T cells are expected to be unresponsive to normal cell culture proteins, as our baseline data indicated. We therefore considered scenarios whereby USSN might initiate the activation of T cells without additional stimuli. Superantigens activate T cells by, generally, crosslinking the T cell receptor (TCR) to MHC class II receptors, as occurs with SEB for example,[47] while anti-CD3 and anti-TCRαβ mitogenic antibodies activate T cells by directly engaging the TCR:CD3 complex.[48] We probed the 'cross-linking' possibility for USSN by reducing the proportion of cells in culture that were positive for MHC class II receptors. These receptors are ubiquitous on APCs such as B cells and monocytes, but occur on only a minority of T cells ($6.01 \pm 2.84\%$ of CD3^{+} T cells) and some NK cells (9.3-37.7%).[49,50] We therefore depleted PBMCs of monocytes (Figure S4) and first confirmed that this led to a significant decrease in the percentage of CD4 T cells positive for CD25 or CD69 after treatment with SEB ($30.1 \pm 4.0\%$ (PBMC) versus $18.5 \pm 5.1\%$ (monocyte-deplete PBMC) for CD25 and $42.4 \pm 5.8\%$ (PBMC) versus $28.2 \pm 4.5\%$ (monocyte-deplete PBMC) for CD69). However, with USSN challenge there was no such decrease of these markers on CD4 T cells in monocyte-depleted cultures ($21.5 \pm 8.6\%$ (PBMC) versus $23.3 \pm 6.5\%$ (monocyte-deplete PBMC) for CD25 and $52.7 \pm 13.4\%$ (PBMC) versus $68.5 \pm 12.6\%$ (monocyte-deplete PBMC) for CD69). Indeed, CD25 and CD69 on CD8 T cells, which are also known to cross-link superantigen to MHC class II receptors,[47] was significantly higher in the monocyte-depleted cultures compared to that in PBMC cultures ($p < 0.005$, Figure 3b versus Figure 7a). Collectively, this indicated that, unlike for SEB, USSN-induced activation of T cells does not require a bridging (i.e., cross-linking) cell expressing the MHC class II receptor and may therefore be via direct T cell-particle interaction. To confirm this, we investigated the impact of USSN on Jurkat cells, which have a CD4 phenotype and do not express MHC class II receptors.[51] Despite high basal CD69 levels, exposure to USSN further increased the percentage of CD69 positive cells whereas SEB, which cannot be cross-lined and bind the TCR sequence

16

on Jurkat cells,[52] had no such effect (Figure 7b). We therefore conclude that USSN activate T cells directly and that the presence of other cells, such as APCs, is not necessary and may actually decrease induced activation, presumably due to competition for cell surface binding and/or uptake of USSN.

Finally, we investigated whether non-silica based ultrasmall particles were also capable of inducing T cell activation. Iron hydroxide nanoparticles (IHNP) of 4.4 ± 0.5 nm median diameter (Figure 8c) and a zeta-potential of -40.0 ± 2.0 mV at pH 6.5 were added at 800 μM Iron$_{TOTAL}$ to complete tissue culture medium (as used for the USSN work) or to a basic salt solution which minimizes agglomeration of the iron hydroxide particles.[53] Ultrasmall IHNP did not significantly induce CD25 or CD69 on T cells in either medium, unlike USSN (Figure 7d,e). Whether the difference in zeta-potential or surface composition between USSN and IHNP is responsible for their differential T cell effects is not clear, but the results indicate that ultrasmall nanoparticle-induction of T cell activation is restricted to certain particle types which, at least, includes USSN.
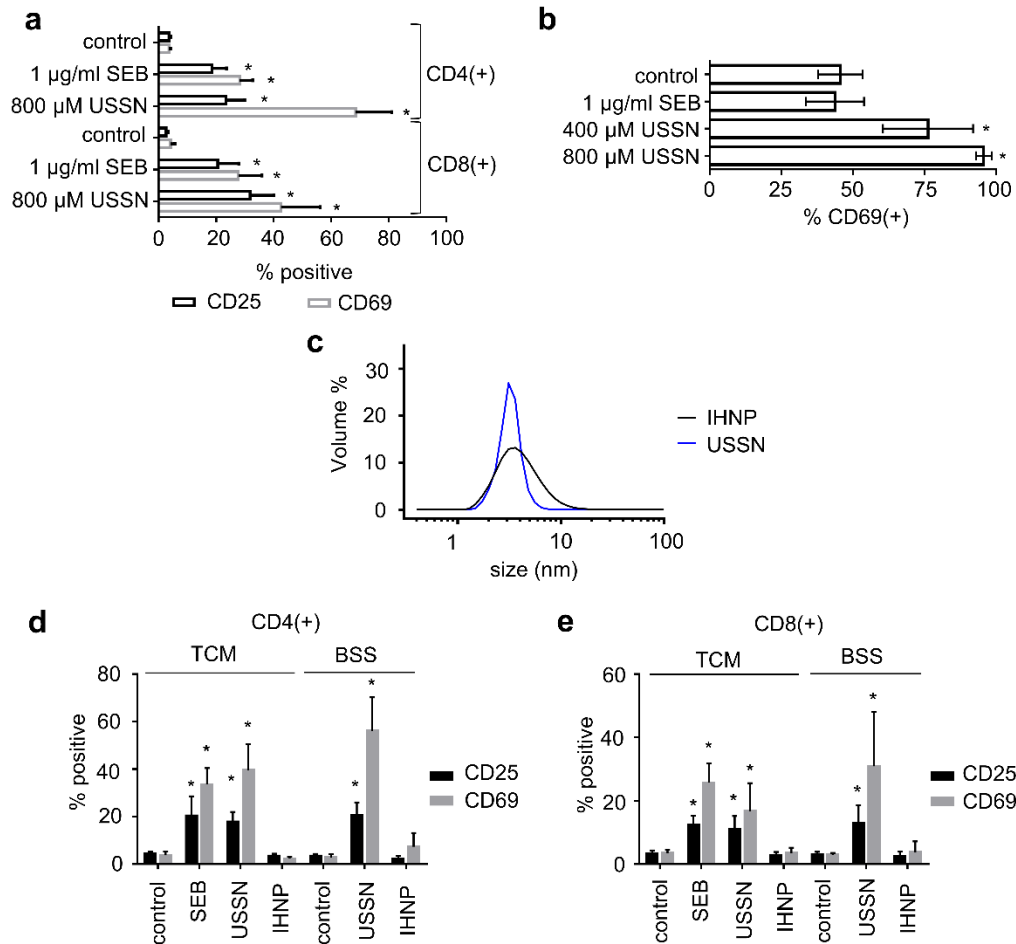
Figure 7. The lack of requirement of APCs in USSN-induced T cell activation and the lack of effect of iron hydroxide nanoparticles on T cell activation. a. The effect of USSN on CD25 and CD69 expression on T cells in enriched T cell cultures. Data represent the means ± standard deviation for 6 donors. (* denotes significance compared to the control, paired T-test, $p < 0.05$.) **b**. The effect of USSN on Jurkat cell line CD69 expression. Data shown represent the means ± standard deviation for 3 independent replicates. (* denotes significant compared to the control, unpaired T-test, $p < 0.05$.) **c.** Size of iron hydroxide nanoparticles in water versus USSN. **d-e**. The effect of IHNP and USSN on CD25 and CD69 expression on CD4 and CD8 T cells in PBMC cultures suspended in TCM and BSS. Data shown represent the means ± standard deviation for 8 donors. (* denotes significance compared to the control in the specific media, one-way ANOVA, $p < 0.05$.)

Conclusions

Ultrasmall nanoparticles of silica are toxic to mononuclear cells, but, additionally and independently, are

potent inducers of cell surface CD25 and CD69 for both T helper (CD4) and CD8 T cells. Our data suggest

that the interaction is direct – between the particle and the T cell – and does not physically require

18

'intermediary' APCs to bridge or cross-link the interaction. The relatively broad range in size dependency of USSN in T cell activation further supports direct binding: silica particles from 1-2 nm to 7-8 nm in diameter, which have particle volumes from ~4.2 nm^3 to ~268 nm^3, respectively, are unlikely to be capable of cross-linking receptors in a similar fashion so a single point interaction is more plausible. Moreover, the rigid nature of USSN, unlike organic superantigens, would not readily facilitate cross-linking interactions.

In addition to these findings, USSN induced significant secretion of IFN-γ in PBMCs. IFN-γ stimulates increased MHC Class I and Class II expression, antigen presentation and cytokine secretion by APCs, as well as killing by NK cells and neutrophils and the further skewing towards a Th_1 inflammatory T cell phenotype. As such, it is widely considered to be a key mediator of cellular immune responses by initiating multiple factors supporting cellular immunity.[44,54,55]

The T cell stimulatory effect in our work was restricted to USSN, as ultrasmall iron hydroxide nanoparticles did not activate T cells. However, zinc oxide nanoparticles, cobalt nanoparticles and fullerenes have all been shown to induce IFN-γ production,[56-58] so the potential for other ultrasmall nanomaterials to influence T cell responses should not be ignored, especially given known exposure.[59,60] Notwithstanding, the USSN effect appears potent presumably because the particles do not completely agglomerate in complex medium and have a local surface geometry/Si-OH affinity for binding. T cells are not known for particle uptake but particles have been shown to interact with these cells via cell surface adhesion.[28] Whether the T cell activation effect is non-selective or involves specific receptors deserves further scrutiny.

Human exposure levels to USSN have not yet been quantified. However, as noted above, these ultrasmall particles are expected to fractionate from the oral additive/excipient E551 in the digestive process,[7] which could allow for interactions with the luminally-exposed, intestinal intra-epithelial T cells, as occurs with orally delivered anti-CD3 antibodies.[61,62] Biomedical applications, including bioimaging, are another potential exposure to USSN.[2,5] The impact of USSN exposure on immune cell activation in vivo via T cell interactions merits consideration.

Methods/Experimental

USSN dispersion preparation and characterization

Preparation. Amorphous silica nanoparticle dispersions were prepared by diluting aliquots of a concentrated alkaline sodium silicate solution (#338443; Sigma-Aldrich Chemical Co., Gillingham, UK) to 23 mM Si in ultra-high purity water (18 MΩ cm) and adjusting to pH 7 with 4 M HCl. This method produced dispersions of USSN with 3.6 ± 0.5 nm median diameter. To produce dispersions with median diameters of 5.1 ± 0.6 and 7.8 ± 0.7 nm, saline (1.5 M stock) was added at a concentration of 30 and 154 mM NaCl, respectively, immediately after pH adjustment. Dispersions with a median diameter of 16 ± 1.3 nm were prepared by adjusting an alkaline silicate solution at 40 mM Si to pH 7 with 4 M HCl. Dispersions of smaller particles (mean diameter < 2 nm) were prepared by rapidly dropping the pH of an alkaline silicate solution, at 500 mM Si, to 0.9 with concentrated HCl (37%) in the presence of a sucrose stabilizer.[63] These low pH dispersions were neutralized immediately prior to use. All dispersions were aged at room temperature for 12-24 h and analyzed by dynamic light scattering prior to use.

Particle size. Hydrodynamic particle size was determined at room temperature by dynamic light scattering using a Zetasizer NanoZS or NanoZSP (Malvern Instruments, Malvern, UK). Acquisition parameters for silicon dioxide for USSN (refractive index = 1.45, absorption = 0.01) and bernate for iron hydroxide nanoparticles (refractive index = 1.92, absorption = 0.10) in a water matrix (1.0031 cP, refractive index = 1.33) were used, along with a 173° backscatter angle. For each sample, three replicate measurements were recorded and the average volume particle distribution reported as DV0.5, corresponding to the 50% cumulative undersize particle distribution. Zeta-potential of the USSN was determined with the NanoZSP, a capillary cell cuvette (DTS1070) and the Smoluchowski diffusion model with F(κa) = 1.50. USSN dispersions were pH adjusted from 1.5 to 9, or diluted in PBS or RPMI, immediately prior to zeta-potential analysis. For each dispersion, zeta-potential measurements were carried out on three independent preparations, with 3 replicate measurements per preparation.

Dissolution in simple media. USSN persistence under physiological conditions was assessed using a molybdic acid dissolution assay.[64] Orthosilicic acid, but not polymeric silica, is complexed by molybdic acid to form a β-silicomolybdate complex that absorbs at 400-450 nm. Following dilution to 1 mM Si in HEPES buffer (pH 7.4), USSN dissolution was assessed by adding 200 μL molybdic acid reagent (4.93 mM $(NH_4)_6Mo_7O_{24} \cdot 4H_2O$ in 0.15 M H_2SO_4) to 100 μL of the diluted sample in a 96 well plate. After 10 min incubation at room temperature, the absorbance at 405 nm was measured on a Labsystems Multiskan RC V1.5-0 plate reader (ThermoScientific, UK). A calibration curve was similarly generated by diluting aliquots of SiF_4 silicon standard (1,000 mg/kg Si; Sigma-Aldrich Co) in HEPES buffer.

Particle size and solubility in TCM. The particle size and solubility of USSN were also determined in complex media. Dispersions were passed through 3 or 1,000 kDa MWCO centrifugal ultrafilters (Vivaspin-500, Sartorius Stedim Biotech; 13,000 rpm for 10 min), which have nominal pore sizes of 1-2 or 11 nm, respectively.[65] Total Si analysis (see below) thus revealed the percentages in the dispersion below 1-2 nm (considered soluble), between 1 and 11 nm, and above 11 nm in size.

Total Si analysis of dispersions and their particle-sizing fractions was conducted by inductively coupled plasma - optical emission spectroscopy (ICP-OES) at 251.611 nm on a Jobin Horiba Ultima 2C with a V-groove nebulizer (Instrument SA, Longjumeau, France), using a flow rate of 0.83 mL/min. Samples were diluted with a pH 10 NaOH solution prior to analysis. Calibration solutions (0.2-70 ppm) were similarly prepared from a SiF_4 silicon standard (Sigma-Aldrich Chemical Co).

^{29}Si NMR spectroscopy was used to characterize USSN dispersions that were prepared as described above except from isotopically-enriched potassium silicate solutions obtained by dissolving [29]SiO_2 (Isonics, 99.35 atom% [29]Si) in an aqueous KOH solution at 170 °C for 24 h in a PTFE-lined pressure vessel. Spectra were acquired at 25 °C on a Bruker AMX500 spectrometer (99.35 MHz) with an Si-free probe and 10 mm O.D. Kel-F sample tube, employing 3600 π/2 pulses and a 53 s interpulse period.

Iron hydroxide nanoparticles synthesis. Iron hydroxide nanoparticles coated with adipate and tartrate were prepared as described previously.[66] Briefly, the pH of an acidic solution containing iron (III) chloride and organic acids was increased to pH 7.4 with NaOH while agitating. The dispersion was dried at 40 °C and, prior to cellular experiments, the iron hydroxide nanoparticles were dispersed in a stock dispersion at 40 mM Fe and particle size was measured by DLS.

Theoretical modelling

Supplementary Fig 1 was created by aggregating a primary $(SiO_2)_{24}$ cluster, which had been previously DFT optimized in a hydrated environment.[25] The smaller clusters were aggregated by eye and allowed to relax locally using the Monte-Carlo algorithm in CrystalMaker®.[67] Further relaxation was not performed. The cluster size was determined from extrapolation of the composition of the previous $(SiO_2)_{24}$ cluster, assuming a continuous surface width of 2.8 Å, which was determined from the average distance from a surface (unterminated) oxygen atom to the first fully condensed (Q^4) silicon atom.

Cellular studies

Cell culture. The Jurkat T cell line was acquired from Leibniz-Institut DSMZ-Deutsche Sammlung von Mikroorganismen und Zellkulturen GmbH. Cells were maintained in Roswell Park Memorial Institute (RPMI)-1640 media containing 10% fetal bovine serum (FBS), 0.3 g/L L-glutamine, 1% penicillin-streptomycin (all from Sigma-Aldrich Co).

Human peripheral blood mononuclear cells (PBMC) were isolated from fresh single leukocyte cones (National Blood Service, Cambridge, UK) using density gradient centrifugation. Isolated cells were rested for 2 h and either used as is or stored in freezing medium (10% dimethyl sulfoxide, 50% FBS, 40% RPMI 1640) at -80 °C or in $N_{2(l)}$. Frozen cells were rapidly thawed, washed, and then rested for 2 h before use in RPMI containing 10% FBS, 0.3 g/L L-glutamine, 1% penicillin-streptomycin and 0.01 µg/mL DNase. The enrichment of T cells through monocyte adherence was conducted by adding PBMC cultures (1-2 × 10^6 cells/mL) to a 6 well plate and incubating at 37 °C for >1 h. Non-adherent cells were transferred to a fresh

6 well plate and adherent cells were discarded. After repeating 3 times, cells were counted and enrichment was assessed using flow cytometry. T cell enrichment was also conducted using a pan T cell negative isolation kit (MACS Miltenyl Biotec, #130-096-535) according to manufacturer's specifications. After enrichment, T cells were rested for a minimum of 2 h prior to use. Difference in activation induced in PBMC and enriched T cell cultures was calculated by: (%CDXX$_{EN\ T\ cells}$ - %CDXX$_{PBMC}$)/ %CDXX$_{PBMC}$ x 100%.

Human PBMC assays were approved by the University of Cambridge Human Biology Research Ethics Committee (ref. HBREC.2015.10)

Cell treatments. Treatments were prepared immediately prior to testing. USSN dispersions were prepared as described above and sterile filtered (0.2 µm) prior to addition to RPMI media (#R0883, Sigma-Aldrich Co.). RPMI supplemented with silicic acid was prepared by diluting sodium silicate solution into RPMI, mixing for 5-30 minutes (spiral mixer) and neutralizing with HCl immediately prior to testing. Staphylococcal enterotoxin B (SEB, Sigma Aldrich, #S4881) in RPMI media containing FBS (#F9665, Sigma-Aldrich Co.) was employed as a positive control. Cells suspended in FBS-containing RPMI were subjected to USSN or SEB for 24 h, 48 h or 72 h and then both the cells and medium were collected (for flow cytometric analysis and for IFNγ, IL-10, IL-2 and IL-4 analyses, respectively). For assessing IL-1β levels (via ELISA), cells were rested for 3 h or pre-stimulated with 10 ng/mL lipopolysaccharide. The cells were washed and subjected to USSN or SEB for 3 h. Cultures were washed again, resuspended in TCM, and incubated for another 21 h. Insoluble peptidoglycan from Staphylococcus aureus was used as the positive control.[29] Media were collected for the IL-1β analysis.

Basic Salt Solution (BSS) was prepared as previously described[53] and was comprised of 3.04 g/L piperazine-N,N′-bis(2-ethanesulfonic acid) (PIPES), 7.60 g/L NaCl, 70.74 g/L KCl, 0.12 g/L MgSO$_4$, 0.90 g/L glucose and 0.24 g/L CaCl$_2$ at pH 6.5.

Gene array. PBMC cultures were treated with 150 μM USSN and incubated for 4 h. RNA was collected using an RNeasy Mini kit (Qiagen, #74104) according to manufacturer's suggested protocol and was stored at -80 °C until analysis. Differences in expression were calculated using an R package limma based on the log$_2$ intensities (fold change = average$_{\text{donorsA-C}}$($2^{\log2(\text{USSN}) - \log2(\text{control})}$)). Gene array were data published on the GEO repository, accession number GSE113088. Mean fold changes were uploaded to the ICEPOP software,[29] selecting species (human), fold change threshold (1.5), and the number of random samples (100). Cell population response was plotted by subtype data.

Flow cytometry. Cell proliferation was assessed using a carboxyfluorescein diacetate, succinimidyl ester (CFDA-SE, 90%, Sigma-Aldrich Chemical Co., UK) dilution assay, as previously described.[68] Cells were stained with 0.1 μM CFDA-SE at 10^6 cells/mL for 7 min prior to treatment with USSN. Cells were stained with fluorescent antibodies according to the manufacturer's suggested protocol with minor changes. Surface antibody staining was conducted by adding a fluorescent antibody cocktail to cells in <100 μL PBS + 1% BSA and incubating on ice for 20 min. For the Invitrogen viability marker, cells were pre-stained with the viability dye for 20 min on ice and washed prior to surface staining. For the 7-AAD viability marker, the viability stain was added to the cells after surface antibody staining and cells were incubated at room temperature for 10 min. Antibodies and stains used were CD3-VioGreen (Miltenyi Biotec, #130-096-910), CD3-PE (BD Pharmingen, #555340), CD4-PE (BD Pharmingen, #555347), CD8-APC-Cy7 (BD Pharmingen, #557834), CD25-FITC (BD Pharmingen, #555431), CD69-APC (BD Pharmingen, #555533), CD11c-APC (BD Pharmingen, #559877), CD19-APC-Cy7 (BD Pharmingen, #557791), 7-AAD (Life technologies, #A1310, Biolegend, #420404), and LIVE/DEAD™ Fixable Violet Dead Cell Stain Kit (Invitrogen, #L34955). All cells were washed and then fixed with PBS + 2% paraformaldehyde. Single stained compensation tubes were prepared alongside the fully stained samples. Flow cytometry analyses were conducted immediately thereafter using a Beckman Coulter CYAN ADP flow cytometer, equipped with 405, 488 and 642 nm solid-state lasers and 11 detectors in standard configuration. Beckman Coulter Summit software was used for data acquisition and analysis. The cytometer was calibrated with alignment

beads (Spherotech, USA), and the coefficients of variation for each channel was within the range set by the manufacturer. 400,000 events or the complete suspensions were acquired. All samples were filtered through 35 µM nylon mesh filters immediately prior to analysis. Flow cytometric data files were saved without applying compensation. Spectral overlap was assessed and data analyzed with the use of unstained and single stained compensation cell samples (1 for each fluorophore used). Compensation was applied according to single stains during post-acquisition analysis to minimize spectral overlap using Summit V4.3 software (Beckman Coulter, UK). For flow cytometric data analysis, treated cells were assessed against the untreated control. An example of the gating strategies used can be found in Figures S5-S7.

ELISA. Cytokine analysis was conducted on the cell supernatants using IL-2 (#DY202), IL-4 (#DY204), IL-10 (#DY217B), IFN-γ (#DY285) and IL-1β (#DY201) ELISA kits (all acquired from R&D Systems) according to manufacturer's specifications.

Statistical analysis

Statistical analyses employed are indicated in the figure captions. Unless otherwise stated, data are expressed as means ± standard deviation. Statistical analyses employed included the two-tailed Student T-test, One-way ANOVA and Two-way ANOVA (using GraphPad Prism 6 software), where a P value of > 0.05 was not considered significant. Whether the data followed a sigmoidal dose response curve was assessed using GraphPad Prism 6 software, using the equation $Y=B+(T-B)*X^n/(Ka^n+X^n)$, where B and T correspond to bottom and top plateau intensities, respectively, Ka is the concentration that induces the 50% response, and X and Ka values are raised to the nth power.

Supporting Information

This Supporting Information is available free of charge via the Internet at http://pubs.acs.org.

It includes details of theoretical modeling of USSN, IL-1β production in PBMC cultures treated with LPS and USSN or peptidoglycan, USSN dissolution in cell culture media (0-8 h), cell distribution in monocyte-

deplete PBMC cultures, gating strategies used in flow cytometric analyses, zeta-potential of USSN in RPMI and PBS, gene pathways significantly up or down-regulated in PBMC after USSN treatment.

Acknowledgements

Author contributions

The initial study was envisioned by JP, REH and BV. In vitro studies were led by BV and REH. BV prepared all USSN dispersions and CB prepared the iron hydroxide nanoparticles. BV, RJ, SDK, and NF designed the physicochemical characterization assays and BV conducted all chemical characterizations and the majority of the PBMC based cell assays. LP designed, undertook, and analysed the inflammasome study. HC developed the USSN model of S1. The manuscript was drafted by BV and JJP, all authors contributed to data interpretation, writing and critical review of the manuscript.

Competing interests

HS Pharma sponsored BV's Ph.D. studentship at MRC EWL and PDF at Lakehead University. The MRC has filed patent applications associated with this work and the IP has been licenced to HS Pharmaceuticals, LLC. Some of the authors are inventors and may receive financial awards to inventors from HSP and the MRC via their licencing structure. Notwithstanding, the authors declare no conflicts of interest.

References

1.   Chen, F.; Ma, K.; Benezra, M.; Zhang, L.; Cheal, S. M.; Phillips, E.; Yoo, B.; Pauliah, M.; Overholtzer, M.; Zanzonico, P.; Seguira, S.; Gonen, M.; Quinn, T.; Wiesner, U.; Bradbury, M. S.,. Cancer-Targeting Ultrasmall Silica Nanoparticles for Clinical Translation: Physicochemical Structure and Biological Property Correlations. Chem. Mater. **2017,** 29, 8766-8779.

2.   Kim, S. E.; Zhang, L.; Ma, K.; Riegman, M.; Chen, F.; Ingold, I.; Conrad, M.; Turker, M. Z.; Gao, M.; Jiang, X., Ultrasmall Nanoparticles Induce Ferroptosis in Nutrient-Deprived Cancer Cells and Suppress Tumour Growth. Nat. Nanotechnol. **2016,** 11, 977-985.

3.   Cifuentes-Rius, A.; Ivask, A.; Das, S.; Penya Auladell, N.; Fabregas, L.; Fletcher, N. L.; Houston, Z. H.; Thurecht, K. J.; Voelcker, N. H., Gold Nanocluster-mediated Cellular Death under Electromagnetic Radiation. ACS Appl. Mater. Interfaces **2017,** 9, 41159-41167.

4.   Huo, M.; Wang, L.; Chen, Y.; Shi, J., Tumor-Selective Catalytic Nanomedicine by Nanocatalyst Delivery. Nat. Commun. **2017,** 8, 357.

5.   Zarschler, K.; Rocks, L.; Licciardello, N.; Boselli, L.; Polo, E.; Garcia, K. P.; De Cola, L.; Stephan, H.; Dawson, K. A., Ultrasmall Inorganic Nanoparticles: State-Of-The-Art and Perspectives for Biomedical Applications. Nanomedicine (N. Y., NY, U. S.) **2016,** 12, 1663-1701.

6.   Lomer, M. C.; Hutchinson, C.; Volkert, S.; Greenfield, S. M.; Catterall, A.; Thompson, R. P.; Powell, J. J., Dietary Sources of Inorganic Microparticles and Their Intake in Healthy Subjects and Patients with Crohn's Disease. Br. J. Nutr. **2004**, 92, 947-955

7.   Peters, R.; Kramer, E.; Oomen, A. G.; Herrera Rivera, Z. E.; Oegema, G.; Tromp, P. C.; Fokkink, R.; Rietveld, A.; Marvin, H. J.; Weigel, S., Presence of Nano-Sized Silica During In Vitro Digestion of Foods Containing Silica as a Food Additive. ACS nano **2012,** 6, 2441-2451.

8.   Jugdaohsingh, R., Silicon and Bone Health. J. Nutr., Health Aging **2007,** 11, 99-110.

9.   Shin, J. H.; Jeon, K.; Kim, J. K.; Kim, Y.; Jo, M. S.; Lee, J. S.; Baek, J. E.; Park, H. S.; An, H. J.; Park, J. D., Subacute Inhalation Toxicity Study of Synthetic Amorphous Silica Nanoparticles in Sprague-Dawley Rats. Inhalation Toxicol. **2017,** 29, 567-576.

10.   Merget, R.; Bauer, T.; Kupper, H. U.; Philippou, S.; Bauer, H. D.; Breitstadt, R.; Bruening, T., Health Hazards Due to the Inhalation of Amorphous Silica. Arch. Toxicol. **2002,** 75, 625-34.

11.   Fruijtier-Pölloth, C., The Toxicological Mode of Action and the Safety of Synthetic Amorphous Silica—A Nanostructured Material. Toxicology **2012,** 294, 61-79.

12.   Fedeli, C.; Selvestrel, F.; Tavano, R.; Segat, D.; Mancin, F.; Papini, E., Catastrophic Inflammatory Death of Monocytes and Macrophages by Overtaking of a Critical Dose of Endocytosed Synthetic Amorphous Silica Nanoparticles/Serum Protein Complexes. Nanomedicine **2013,** 8, 1101-1126.

13.   Mendoza, A.; Torres-Hernandez, J. A.; Ault, J. G.; Pedersen-Lane, J. H.; Gao, D.; Lawrence, D. A., Silica Nanoparticles Induce Oxidative Stress and Inflammation of Human Peripheral Blood Mononuclear Cells. Cell Stress Chaperones **2014,** 19, 777-790.

14.   Hirai, T.; Yoshioka, Y.; Takahashi, H.; Ichihashi, K.; Yoshida, T.; Tochigi, S.; Nagano, K.; Abe, Y.; Kamada, H.; Tsunoda, S., Amorphous Silica Nanoparticles Enhance Cross-Presentation in Murine Dendritic Cells. Biochem. Biophys. Res. Commun. **2012**, 427, 553-556

15.   Malachin, G.; Lubian, E.; Mancin, F.; Papini, E.; Tavano, R., Combined Action of Human Commensal Bacteria and Amorphous Silica Nanoparticles on the Viability and Immune Responses of Dendritic Cells. Clin. Vaccine Immunol. **2017**, 24, e00178-17

16.   Chen, W.; Zhang, Q.; Kaplan, B. L.; Baker, G. L.; Kaminski, N. E., Induced T Cell Cytokine Production Is Enhanced by Engineered Nanoparticles. Nanotoxicology **2014,** 8, 11-23.

17.   Brandenberger, C.; Rowley, N. L.; Jackson-Humbles, D. N.; Zhang, Q.; Bramble, L. A.; Lewandowski, R. P.; Wagner, J. G.; Chen, W.; Kaplan, B. L.; Kaminski, N. E., Engineered Silica Nanoparticles Act as Adjuvants to Enhance Allergic Airway Disease in Mice. Part. Fibre Toxicol. **2013**, 10, 26.

18.   Meldrum, K.; Guo, C.; Marczylo, E. L.; Gant, T. W.; Smith, R.; Leonard, M. O., Mechanistic Insight into the Impact of Nanomaterials on Asthma and Allergic Airway Disease. Part. Fibre Toxicol. **2017,** 14, 45.

19.   Anselmo, A. C.; Mitragotri, S., Nanoparticles in the Clinic. Bioeng. Transl. Med. **2016**, 1, 10-29.

20.   Jugdaohsingh, R.; Brown, A.; Dietzel, M.; Powell, J. J., High-Aluminum-Affinity Silica Is a Nanoparticle That Seeds Secondary Aluminosilicate Formation. PLoS One **2013,** 8, e84397.

21.   Kalia, P.; Brooks, R. A.; Kinrade, S. D.; Morgan, D. J.; Brown, A. P.; Rushton, N.; Jugdaohsingh, R., Adsorption of Amorphous Silica Nanoparticles Onto Hydroxyapatite Surfaces Differentially Alters Surfaces Properties and Adhesion of Human Osteoblast Cells. PloS One **2016,** 11, e0144780.

22.   Casey, W.; Kinrade, S.; Knight, C.; Rains, D.; Epstein, E., Aqueous Silicate Complexes in Wheat, Triticum Aestivum L. Plant, Cell Environ. **2004,** 27, 51-54.

23.   Gary, L. W.; de Jong, B. H. W. S.; Dibble Walter, E., A ^{29}Si NMR Study of Silica Species in Dilute Aqueous Solution. Geochim. Cosmochim. Acta **1982,** 46, 1317-1320.

24.   Meinhold, R.; Rothbaum, H.; Newman, R., Polymerization of Supersaturated Silica Solutions Monitored by Silicon-29 Nuclear Magnetic Resonance. J. Colloid Interface Sci. **1985,** 108, 234-236.

25.   (2012). Silica, Amorphous [MAK Value Documentation, 1991] . In The MAK-Collection for Occupational Health and Safety (eds and). doi:10.1002/3527600418.mb763186e0002

26.   Jelfs, K. E.; Flikkema, E.; Bromley, S. T., Hydroxylation of Silica Nanoclusters $(SiO_2)_M(H_2O)_N$, M= 4, 8, 16, 24: Stability and Structural Trends. Phys. Chem. Chem. Phys. **2013,** 15, 20438-20443.

27.   Napierska, D.; Thomassen, L. C. J.; Lison, D.; Martens, J. A.; Hoet, P. H., The Nanosilica Hazard: Another Variable Entity. Part. Fibre Toxicol. **2010,** 7, 39-39.

28.   Hewitt, R. E.; Vis, B.; Pele, L. C.; Faria, N.; Powell, J. J., Imaging Flow Cytometry Assays for Quantifying Pigment Grade Titanium Dioxide Particle Internalization and Interactions With Immune Cells in Whole Blood. Cytometry, Part A **2017,** 91, 1009-1020.

29.   Pele, L.; Haas, C. T.; Hewitt, R.; Faria, N.; Brown, A.; Powell, J., Artefactual Nanoparticle Activation of the Inflammasome Platform: In Vitro Evidence with a Nano-Formed Calcium Phosphate. Nanomedicine (London, U. K.) **2015,** 10, 1379-1390.

30.   Wijaya, E.; Igarashi, Y.; Nakatsu, N.; Haseda, Y.; Billaud, J.; Chen, Y.; Mizuguchi, K.; Yamada, H.; Ishii, K.; Aoshi, T., Quantifying the Relative Immune Cell Activation from Whole Tissue/Organ-Derived Differentially Expressed Gene Data. Sci. Rep. **2017**, 7, 12847.

31.   Wijaya, E., ICEPOP https://vdynamics.shinyapps.io/icepop/#section-basic (accessed June 18, 2018)

32.   Long, E. O.; Kim, H. S.; Liu, D.; Peterson, M. E.; Rajagopalan, S., Controlling NK Cell Responses: Integration of Signals for Activation and Inhibition. Annu. Rev. Immunol. **2013** 31, 227-258

33.   Zwirner, N. W.; Domaica, C. I., Cytokine Regulation of Natural Killer Cell Effector Functions. Biofactors **2010**, 36, 274-288.

34.   Abbas, A. R.; Baldwin, D.; Ma, Y.; Ouyang, W.; Gurney, A.; Martin, F.; Fong, S.; van Lookeren Campagne, M.; Godowski, P.; Williams, P., Immune Response In Silico (IRIS): Immune-Specific Genes Identified from a Compendium of Microarray Expression Data. Genes Immun. **2005**, 6, 319-331.

35.   Radulovic, K.; Rossini, V.; Manta, C.; Holzmann, K.; Kestler, H. A.; Niess, J. H., The Early Activation Marker CD69 Regulates the Expression of Chemokines and CD4 T Cell Accumulation in Intestine. PloS One **2013,** 8, e65413.

36.   Schwartzberg, P. L.; Mueller, K. L.; Qi, H.; Cannons, J. L., SLAM Receptors and SAP Influence Lymphocyte Interactions, Development and Function. Nat. Rev. Immunol. **2009,** 9, 39-46.

37.   Geginat, J.; Paroni, M.; Maglie, S.; Alfen, J. S.; Kastirr, I.; Gruarin, P.; De Simone, M.; Pagani, M.; Abrignani, S., Plasticity of Human CD4 T Cell Subsets. Front. Immunol. **2014**, 67.

38.   Brownlie, R. J.; Zamoyska, R., T Cell Receptor Signalling Networks: Branched, Diversified and Bounded. Nat. Rev. Immunol. **2013**, 13, 257-269.

39.   D'Souza, W. N.; Lefrançois, L., IL-2 Is Not Required for the Initiation of CD8 T Cell Cycling But Sustains Expansion. J. Immunol. **2003,** 171, 5727-5735.

40.   Malek, T. R.; Castro, I., Interleukin-2 Receptor Signaling: At the Interface Between Tolerance and Immunity. Immunity **2010,** 33, 153-165.

41.   Clausen, J.; Vergeiner, B.; Enk, M.; Petzer, A. L.; Gastl, G.; Gunsilius, E., Functional Significance of the Activation-Associated Receptors CD25 and CD69 on Human NK-Cells and NK-Like T-Cells. Immunobiology **2003,** 207, 85-93.

42. Mackay, L. K.; Braun, A.; Macleod, B. L.; Collins, N.; Tebartz, C.; Bedoui, S.; Carbone, F. R.; Gebhardt, T., Cutting Edge: CD69 Interference With Sphingosine-1-Phosphate Receptor Function Regulates Peripheral T Cell Retention. J. Immunol. **2015,** 194, 2059-2063.

43. Geginat, J.; Paroni, M.; Maglie, S.; Alfen, J. S.; Kastirr, I.; Gruarin, P.; De Simone, M.; Pagani, M.; Abrignani, S., Plasticity of Human CD4 T Cell Subsets. Front. Immunol. **2014**, 67.

44. Commins, S. P.; Borish, L.; Steinke, J. W., Immunologic Messenger Molecules: Cytokines, Interferons, and Chemokines. J. Allergy Clin. Immunol. **2010**, 125, S53-S72

45. Lehman, S. E.; Mudunkotuwa, I. A.; Grassian, V. H.; Larsen, S. C., Nano–Bio Interactions of Porous and Nonporous Silica Nanoparticles of Varied Surface Chemistry: A Structural, Kinetic, and Thermodynamic Study of Protein Adsorption from RPMI Culture Medium. Langmuir **2016**, 32, 731-742.

46. Belton, D. J.; Deschaume, O.; Perry, C. C., An Overview of the Fundamentals of the Chemistry of Silica With Relevance to Biosilicification and Technological Advances. FEBS J. **2012**, 279, 1710-1720.

47. Fleischer, B.; Gerardy-Schahn, R.; Metzroth, B.; Carrel, S.; Gerlach, D.; Köhler, W., An Evolutionary Conserved Mechanism of T Cell Activation by Microbial Toxins. Evidence for Different Affinities of T Cell Receptor-Toxin Interaction. J. Immunol. **1991**, 146, 11-17.

48. Minguet, S.; Swamy, M.; Alarcón, B.; Luescher, I. F.; Schamel, W. W. A., Full Activation of the T Cell Receptor Requires Both Clustering and Conformational Changes at CD3. Immunity **2007**, 26, 43-54.

49. Pasiarski, M.; Grywalska, E.; Kosmaczewska, A.; Góźdź, S.; Steckiewicz, P.; Garus, B.; Hymos, A.; Bilski, M.; Zgurski, M.; Roliński, J., Assessment of Peripheral Blood and Bone Marrow T, NK, NKT and Dendritic Cells in Patients with Multiple Myeloma. Postepy Hig. Med. Dosw. **2015**, 69. 1435-1442

50. D'Orazio, J.; Stein-Streilein, J., Human natural killer (NK) Cells Present Staphylococcal Enterotoxin B (SEB) to T Lymphocytes. Clin. Exp. Immunol. **1996**, 104, 366-373.

51. Holling, T. M.; Schooten, E.; Langerak, A. W.; van den Elsen, P. J., Regulation of MHC Class II Expression in Human T-Cell Malignancies. Blood **2004**, 103, 1438-1444.

52. Hayworth, J.; Kasper, K.; Leon-Ponte, M.; Herfst, C.; Yue, D.; Brintnell, W.; Mazzuca, D.; Heinrichs, D.; Cairns, E.; Madrenas, J., Attenuation of Massive Cytokine Response to the Staphylococcal Enterotoxin B Superantigen by the Innate Immunomodulatory Protein Lactoferrin. Clin. Exp. Immunol. **2009,** 157, 60-70.

53. Pereira, D. I.; Lederer, B.; Powell, J. J., A Balanced Salt Solution That Prevents Agglomeration of Nano Iron Oxo-Hydroxides in Serum-Free Cellular Assays. Mater. Res. Express **2015**, 2, 015403.

54. Billiau, A.; Matthys, P., Interferon-γ: A Historical Perspective. Cytokine Growth Factor Rev. **2009,** 20, 97-113.

55. Schroder, K.; Hertzog, P. J.; Ravasi, T.; Hume, D. A., Interferon-γ: An Overview of Signals, Mechanisms and Functions. J. Leukocyte Biol. **2004,** 75, 163-189.

56. Hanley, C.; Thurber, A.; Hanna, C.; Punnoose, A.; Zhang, J.; Wingett, D. G., The Influences of Cell Type and ZnO Nanoparticle Size on Immune Cell Cytotoxicity and Cytokine Induction. Nanoscale Res. Lett. **2009,** 4, 1409-1420.

57. Liu, Y.; Jiao, F.; Qiu, Y.; Li, W.; Qu, Y.; Tian, C.; Li, Y.; Bai, R.; Lao, F.; Zhao, Y., Immunostimulatory Properties and Enhanced TNF-A Mediated Cellular Immunity for Tumor Therapy by C60 (OH) 20 Nanoparticles. Nanotechnology **2009,** 20, 415102.

58. Petrarca, C.; Perrone, A.; Verna, N.; Verginelli, F.; Ponti, J.; Sabbioni, E.; Di Giampaolo, L.; Dadorante, V.; Schiavone, C.; Boscolo, P., Cobalt Nano-Particles Modulate Cytokine In Vitro Release by Human Mononuclear Cells Mimicking Autoimmune Disease. Int. J. Immunopathol. Pharmacol. **2005,** 19, 11-14.

59. Sirignano, M.; Conturso, M.; Magno, A.; Di Iorio, S.; Mancaruso, E.; Vaglieco, B. M.; D'Anna, A., Evidence of Sub-10 nm Particles Emitted from a Small-Size Diesel Engine. Exp. Therm. Fluid Sci. **2018**, 95, 60-64.

60. Pedata, P.; Stoeger, T.; Zimmermann, R.; Peters, A.; Oberdörster, G.; D'Anna, A., Are We Forgetting the Smallest, Sub 10 nm Combustion Generated Particles? Part. Fibre Toxicol. **2015**, 12, 34.

61.   Mowat, A. M.; Agace, W. W., Regional Specialization Within the Intestinal Immune System. Nat. Rev. Immunol. **2014,** 14, 667.

62.   Ochi, H.; Abraham, M.; Ishikawa, H.; Frenkel, D.; Yang, K.; Basso, A. S.; Wu, H.; Chen, M.-L.; Gandhi, R.; Miller, A., Oral CD3-Specific Antibody Suppresses Autoimmune Encephalomyelitis by Inducing CD4+ CD25− LAP+ T Cells. Nat. Med. (N. Y., NY, U. S.) **2006,** 12, 627.

63.   Bastos, C. A. P.; Powell, J. J.; Faria, N. J. R.; Vis, B. M., Materials and Methods Relating to Stabilised Polymeric Silicate Compositions. WO Patent WO2015121666 A1 application 14 Feb 2014.

64.   Alexander, G. B.; Heston, W.; Iler, R. K., The Solubility of Amorphous Silica in Water. J. Phys. Chem. **1954,** 58, 453-455.

65.   Guo, L.; Santschi, P. H., Ultrafiltration and Its Applications to Sampling and Characterisation of Aquatic Colloids. IUPAC Ser. Anal. Phys. Chem. Environ. Syst. **2007,** 10, 159.

66.   Powell, J. J.; Bruggraber, S. F. A.; Faria, N. J. R.; Pereira, D. I. A., Ligand Modified Poly Oxo-Hydroxy Metal Ion Materials, Their Uses and Processes for Their Preparation. US Patent US805846B2 granted 15 Nov 2011

67.   Palmer, D., CrystalDiffract®: A Powder Diffraction Program for Mac and Windows. , www.crystalmaker.com, 2017.

68.   Lyons, A. B.; Parish, C. R., Determination of Lymphocyte Division by Flow Cytometry. J. Immunol. Methods **1994**, 171, 131-137.

69.   Kobayashi, M.; Juillerat, F.; Galletto, P.; Bowen, P.; Borkovec, M., Aggregation and Charging of Colloidal Silica Particles: Effect of Particle Size. Langmuir **2005,** 21, 5761-5769.